

# Structures of Bare and Hydrated $[\text{Pb}(\text{AminoAcid-H})]^+$ Complexes Using Infrared Multiple Photon Dissociation Spectroscopy

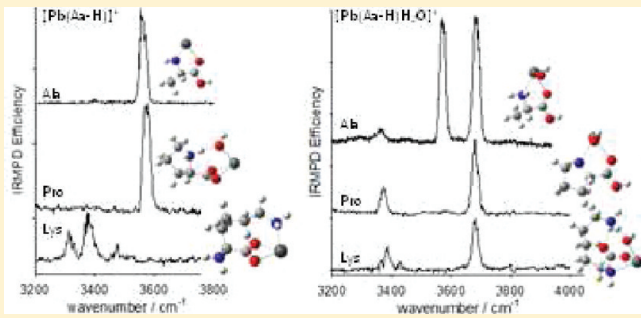
Michael B. Burt,<sup>†</sup> Sarah G. A. Decker,<sup>†</sup> Chad G. Atkins,<sup>†</sup> Mark Rowsell,<sup>†</sup> André Peremans,<sup>‡</sup> and Travis D. Fridgen<sup>\*†</sup>

<sup>†</sup>Department of Chemistry, Memorial University of Newfoundland, St. John's, Newfoundland and Labrador, Canada, A1B 3X7

<sup>‡</sup>The Research Centre in Physics of Matter and Radiation, University of Namur (FUNDP), rue de Bruxelles 61, B-5000 Namur, Belgium

Supporting Information

**ABSTRACT:** Infrared multiple-photon dissociation (IRMPD) spectroscopy was used to determine the gas-phase structures of deprotonated  $\text{Pb}^{2+}$ /amino acid (Aa) complexes with and without a solvent molecule present. Five amino acid complexes with side chains containing only carbon and hydrogen (Ala, Val, Leu, Ile, Pro) and one with a basic side chain (Lys) were compared. These experiments demonstrated that all  $[\text{Pb}(\text{Aa-H})]^+$  complexes have  $\text{Pb}^{2+}$  covalently bound between the amine nitrogen and carbonyl oxygen. The nonhydrated complexes containing Ala, Val, Leu, Ile, and Pro are amine-deprotonated, whereas the one containing Lys is deprotonated at its carboxylic acid. The difference is attributed to the polar and basic side chain of lysine, which helps stabilize  $\text{Pb}^{2+}$ . IRMPD spectroscopy was also performed on the monohydrated analogues of the  $[\text{Pb}(\text{Aa-H})]^+$  complexes. The  $[\text{Pb}(\text{Aa-H})\text{H}_2\text{O}]^+$  complexes, where Aa = Ala, Val, Leu, and Ile, exhibited two N–H stretches as well as a carboxylic acid O–H and a PbO–H stretch. Hence, their structures are monohydrated versions of the amine-deprotonated  $[\text{Pb}(\text{Aa-H})]^+$  complexes where a proton transfer has occurred from the lead-bound water to the deprotonated amine. The IRMPD spectrum and calculations suggest that  $[\text{Pb}(\text{Pro-H})\text{H}_2\text{O}]^+$  has a hydrated carboxylate salt structure. The structure of  $[\text{Pb}(\text{Lys-H})\text{H}_2\text{O}]^+$  was also carboxyl-deprotonated, but  $\text{Pb}^{2+}$  is bound to the carbonyl oxygen and the amine nitrogen, with one of the protons belonging to the water transferred to the basic side chain. This results in an intramolecular hydrogen bond that does not absorb in the region of the spectrum probed in these experiments. The IRMPD spectra and structural characterizations were confirmed and aided by infrared spectra calculated at the B3LYP/6-31+G(d,p) level of theory and 298 K enthalpies and Gibbs energies using the MP2(full)/6-311++G(2d,2p) method on the B3LYP geometries.



## 1. INTRODUCTION

Heavy metal ions, such as lead(II), are known to cause harmful chemical reactions within humans. For instance, they have been associated with the formation of toxic aggregates involved with Alzheimer's disease as well as effects related to hypertension and anemia.<sup>1</sup> The degree of this toxicity depends on the efficiency of lead(II) complex formation with proteins or peptides, which can act as antitoxins by effectively removing the metal ions through chelation.<sup>1–5</sup> Despite the implications of lead(II)–peptide complexes in biochemistry, spectroscopic and structural information on these species remains incomplete. Recent electrospray ionization mass spectrometry (ESI-MS) studies of lead(II)/amino acid solutions demonstrated that the complexes are deprotonated and of the form  $[\text{Pb}(\text{Aa-H})]^+$  (Aa = amino acid), but the actual structures of the complexes were not determined.<sup>6–8</sup> In this Article, infrared multiple-photon dissociation (IRMPD) spectroscopy is used to structurally characterize  $[\text{Pb}(\text{Aa-H})]^+$  and  $[\text{Pb}(\text{Aa-H})\text{H}_2\text{O}]^+$  complexes for five amino acids with nonpolar side chains (proline (Pro), alanine (Ala), valine (Val), leucine (Leu), and isoleucine (Ile)) and one amino acid containing a polar and basic side chain (lysine (Lys)).

IRMPD spectroscopy is one form of consequence spectroscopy that allows structural features of ions to be directly determined.<sup>9–11</sup> This technique couples a mass spectrometer to a tunable infrared (IR) source such as the widely used tabletop OPO/OPA lasers<sup>9–17</sup> or the free electron lasers (FELs) at CLIO<sup>18</sup> or FELIX.<sup>19</sup> If the impinging radiation is in resonance with a vibrational mode of the isolated ion, then the ion will absorb a photon. This vibrational energy is rapidly redistributed, allowing multiple photons to be absorbed at the same wavelength. Once the ion has accumulated enough internal energy that it has significantly surpassed its dissociation threshold, fragmentation of the ion is observed. By scanning over a range of wavelengths, an ion's vibrational spectrum is revealed. The assignment of the vibrational modes is often supported by comparing them to computed IR absorption spectra from electronic structural calculations, allowing for the structure of the complexes to be determined.

**Received:** July 18, 2011

**Revised:** August 24, 2011

**Published:** August 29, 2011

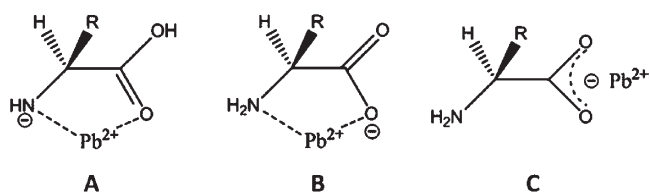


**Figure 1.** Three main types of complexes formed between  $\text{Pb}^{2+}$  and the conjugate bases of amino acids.

The appeal of gas-phase ion techniques such as IRMPD, blackbody IR radiative dissociation (BIRD), and collisionally induced dissociation (CID) stems from their ability to explore the intrinsic properties of the ion without the complication of bulk solvent. The activity and function of cationic amino acid complexes are partially dictated by the distribution of electrostatic forces throughout the molecule. In the condensed phases, for example, solvents such as water can alter the conformation of amino acids and proteins.<sup>20</sup> Studying the gas-phase ion and comparing to solution-phase data can provide insight into the role of the solvents themselves. In the present study, the solvent absence allows for a better understanding of the interactions between lead(II) and the deprotonated amino acid binding sites as well as the result of singly hydrating  $[\text{Pb}(\text{Aa-H})]^+$ .

Recently, a large volume of work has been directed at determining the structures of stable gas-phase amino acid complexes through microsolvation,<sup>21–33</sup> dimerization,<sup>13,34–40</sup> or metal chelation.<sup>13,41–59</sup> The majority of research has focused on  $[\text{M(Aa)}]^{+2+}$ , where M is an alkali or alkaline earth metal. The p-block amino acid complexes, however, have been largely ignored. Unlike other p-block metals, lead is known to complex with every amino acid, making it an excellent starting point for the investigation of peptide–ion complexes.<sup>7</sup> The dominant gas-phase lead–amino acid complexes formed by electrospray are deprotonated, and these have been the focus of our research.  $[\text{M(Aa-H)}]^+$  complexes are not as well characterized as  $[\text{M(Aa)}]^+$  or  $[\text{M(Aa)}]^{2+}$  structures, although Rogalewicz et al. have rigorously explored the structure and fragmentation pathways of  $[\text{Zn}(\text{Gly-H})]^+$  using low-energy CID,<sup>60–63</sup> and prior work by Atkins et al. used IRMPD to characterize the structure of  $[\text{Pb}(\text{Gly-H})]^+$ .<sup>12</sup> Atkins'  $[\text{Pb}(\text{Gly-H})]^+$  IRMPD spectrum revealed a strong IR absorption band around  $3540\text{ cm}^{-1}$ , which was assigned to the carboxylic acid O–H stretch. The proton lost in  $[\text{Pb}(\text{Gly-H})]^+$  must therefore belong to the amine group because the carboxylic acid functional group remains intact. This was supported by DFT and ab initio electronic structure calculations that demonstrated that the lowest energy structure of  $[\text{Pb}(\text{Gly-H})]^+$  is one where  $\text{Pb}^{2+}$  is bound through a covalent interaction between the deprotonated amine group and the carbonyl oxygen of the carboxylic acid group (A in Figure 1A). Further IRMPD spectroscopy experiments on  $[\text{Pb}(\text{Gly-H})\text{H}_2\text{O}]^+$ , its isotopomer  $[\text{Pb}(\text{Gly-H})\text{H}_2^{18}\text{O}]^+$ ,  $[\text{Pb}(\text{Gly-H})\text{CH}_3\text{OH}]^+$ , and the glycine ethyl ester helped to confirm the structure of  $[\text{Pb}(\text{Gly-H})]^+$ .  $\text{Pb}^{2+}$  can interact with deprotonated amino acids in several ways. Figure 1 shows three  $[\text{Pb}(\text{Aa-H})]^+$  conformers. A is amine-deprotonated, whereas B and C are carboxyl-deprotonated.  $\text{Pb}^{2+}$  binds between the amine group and the carboxylic acid in A and B and lies between the two oxygens in C.<sup>12</sup> The following discussion will reveal that the sites of deprotonation and  $\text{Pb}^{2+}$  binding are strongly dependent on the nature of the amino acid side chain.

This Article extends the characterization of deprotonated lead-amino acid structures by using IRMPD spectroscopy to provide spectra for bare and monohydrated lead complexes with six amino acids containing side chains of varying polarity and basicity (Ala, Val, Leu, Ile, Pro, and Lys). Electronic structure calculations are also used to help assign structures determined from the IRMPD spectra by comparing them to computed IR spectra. Furthermore, the manner in which side chains stabilize these complexes will also be presented.

## 2. METHODS

**2.1. IRMPD Spectroscopy.**  $[\text{Pb}(\text{Aa-H})]^+$  complexes were prepared by mixing  $\sim 0.1\text{ mM}$   $\text{Pb}(\text{NO}_3)_2$  ( $>99\%$ , Fluka Chemika) and  $0.1\text{ mM}$  Aa (Aa = Ala, Val, Leu, Ile, Pro, and Lys) (Nutritional Biochemicals) in a 50/50 mixture of  $18.2\text{ M}\Omega$  water (Millipore) and methanol (99.8%, ACP Chemicals). The  $[\text{Pb}(\text{Aa-H})]^+$  solution was flowed at  $100\text{ }\mu\text{L/h}$  into an Apollo II ion source of a Bruker Apex Qe 7 T Fourier transform ion cyclotron resonance (FTICR) mass spectrometer. The voltage across the source exit capillary was 294 V. The  $[\text{Pb}(\text{Aa-H})]^+$  ions were then mass selected by a quadrupole mass filter and allowed to accumulate in a hexapole collision cell for 0.8 to 2 s before being transferred to the ICR cell. Once in the ICR cell, the ions were irradiated using a potassium titanyl phosphate optical parametric oscillator (KTP OPO) for 2–7 s over the spectroscopic range of  $3200\text{--}4000\text{ cm}^{-1}$  at intervals of  $1.5\text{ cm}^{-1}$ . Two to six mass spectra were averaged per wavelength step. IRMPD spectra were prepared by plotting the IRMPD yield as a function of the OPO radiation frequency. The IRMPD yield is defined as the base 10 logarithm of the normalized precursor ion intensity.

The preparation of solvated complexes involved an extra step.<sup>64</sup> The collision cell has both an argon gas inlet line and a vapor inlet line. The argon flow is minimized, whereas the desired solvent is added to the collision cell through the vapor inlet by opening a microvalve. The solvents were degassed by a series of freeze–pump–thaw cycles prior to use.

The KTP OPO is pumped collinearly using a brilliant B Nd: YAG laser (Big Sky Laser). The pump source is a 1064 nm fundamental line emitted in 6 ns (850 mJ) pulses at 10 Hz through a dichroic cavity mirror; this input mirror is highly reflective with respect to the signal wavelength (1.528 to  $2.128\text{ }\mu\text{m}$ ). The KTP crystal ( $8 \times 12 \times 25\text{ mm}$ ) is enclosed in an OPO cavity, which is only resonant with the signal wave. The output mirror is transparent at the pump wavelength and the idler wavelength ( $2.128$  to  $3.500\text{ }\mu\text{m}$ ) but is 30% reflective with respect to the signal wavelength. The dichroic input and output mirrors allow the KTP OPO to produce two perpendicular beams: the signal and idler. The idler beam is used for near-IR spectroscopy between  $2.128$  and  $3.500\text{ }\mu\text{m}$ , although in practice the useful range for IRMPD spectroscopy experiments is approximately  $2.5$  to  $3.13\text{ }\mu\text{m}$  ( $4000\text{--}3200\text{ cm}^{-1}$ ). The OPO (Euroscan) has a  $3\text{ cm}^{-1}$  bandwidth, and the output pulse varies as a function of the wavelength used. The maximum efficiency occurs at  $2.6\text{ }\mu\text{m}$ , where the conversion efficiency for an 800 mJ pump pulse is 20%, producing a 60 mJ idler pulse. The idler output then decreases somewhat linearly as wavelength increases; energy output above  $3.2\text{ }\mu\text{m}$  is  $\sim 10\text{ mJ}$ , and energy output ceases between  $3.4$  and  $3.5\text{ }\mu\text{m}$ . The idler beam divergence ( $0.5^\circ$ ) and astigmatism are corrected using a spherical Au mirror ( $f = 3000\text{ mm}$ ) as well as a cylindrical ( $f = 400\text{ mm}$ )  $\text{CaF}_2$  lens. The beam is then focused into the ICR cell by a 200 mm

$\text{CaF}_2$  focal length lens. The KTP OPO idler beam is transmitted into the ICR cell through a path purged of  $\text{CO}_2$  and  $\text{H}_2\text{O}$ . The radiation enters the ICR vacuum chamber through a  $\text{BaF}_2$  window and then irradiates the ion packet in the ICR cell. The ICR cell itself is surrounded by a homemade heating jacket thermalized near 100 °C. This facilitates dissociation of the lead complexes and increases the observed signal intensities.

**2.2. Calculations.** The Gaussian 09 software package was employed for all calculations.<sup>65</sup> Roughly 20–40 unique conformers were considered for each complex, but for clarity only 3–7 of the lowest energy minima are reported here for each structure. Each set of conformers was created by varying the sites of deprotonation and lead chelation as well as by altering bond and torsional angles to maximize hydrogen bonding or to relieve molecular strain. Geometry optimizations and harmonic frequency calculations were performed on every conformer using B3LYP density functional theory in conjunction with the LANL2DZ basis set and relativistic core potential for lead and the 6-31+G(d,p) basis set for all other atoms. This method is abbreviated here as B3LYP/6-31+G(d,p), although it should be remembered that the LANL2DZ basis set is used for lead. The vibrational modes were scaled by a factor of 0.955 to compare with the experimental IRMPD spectra.<sup>12,13</sup>

Single-point energy calculations were performed on each optimized structure at the MP2 level of theory using the same basis set and core potential for lead and the larger 6-311++G(2d,2p) basis set for the other atoms. The 298 K Gibbs energies and enthalpies are reported as MP2(full)/6-311++G(2d,2p)//B3LYP/6-31+G(d,p). Like the B3LYP method, this is an abbreviation that omits the LANL2DZ basis set, although it was used for the lead atom.

Thermodynamic data for the bare and hydrated Pro and Ala complexes were also calculated by replacing the LANL2DZ basis set with the SDD effective core potential (ECP) for lead; geometry optimizations as well as single point energies were recalculated using this approach.<sup>66</sup> The MP2(full)/6-311++G(2d,2p)//B3LYP/6-31+G(d,p) method was still employed for all other atoms. This change in methodology arose from an observed discrepancy, discussed in more detail below, between the experimental results and the global minimum structure of  $[\text{Pb}(\text{Pro-H})]^+$  calculated by the LANL2DZ method.

Transition states were also determined for isomerization reactions involving  $[\text{Pb}(\text{Pro-H})]^+$ ,  $[\text{Pb}(\text{Ala-H})]^+$ ,  $[\text{Pb}(\text{Pro-H}-\text{H}_2\text{O})]^+$ , and  $[\text{Pb}(\text{Ala-H})\text{H}_2\text{O}]^+$ . These were authenticated by the presence of one imaginary vibrational mode that corresponds to the correct reaction coordinate.

### 3. RESULTS AND DISCUSSION

**3.1. Comparison of  $[\text{Pb}(\text{Aa-H})]^+$  and  $[\text{Pb}(\text{Aa-H})\text{H}_2\text{O}]^+$  Infrared Spectra.** The IRMPD spectra in the 3200–3800  $\text{cm}^{-1}$  range for  $[\text{Pb}(\text{Aa-H})]^+$  are compared in Figure 2. In each case, the only fragmentation caused by absorption of the KTP OPO laser was  $\text{H}_2\text{O}$  loss, although  $[\text{Pb}(\text{Val-H})]^+$  also lost a small amount of CO over its O–H stretch region (12% of the  $\text{H}_2\text{O}$  loss).

The nonhydrated complexes containing Ala, Val, Leu, and Ile exhibit similar absorbance patterns. Each spectrum contains a weak absorbance in the N–H stretch region at approximately 3410–3440  $\text{cm}^{-1}$  and a strong absorbance centered around 3560  $\text{cm}^{-1}$  in the O–H stretch region. The weaker band is assigned as an N–H stretch, whereas the strong one is the carboxylic acid O–H stretch. The spectrum of  $[\text{Pb}(\text{Pro-H})]^+$  is

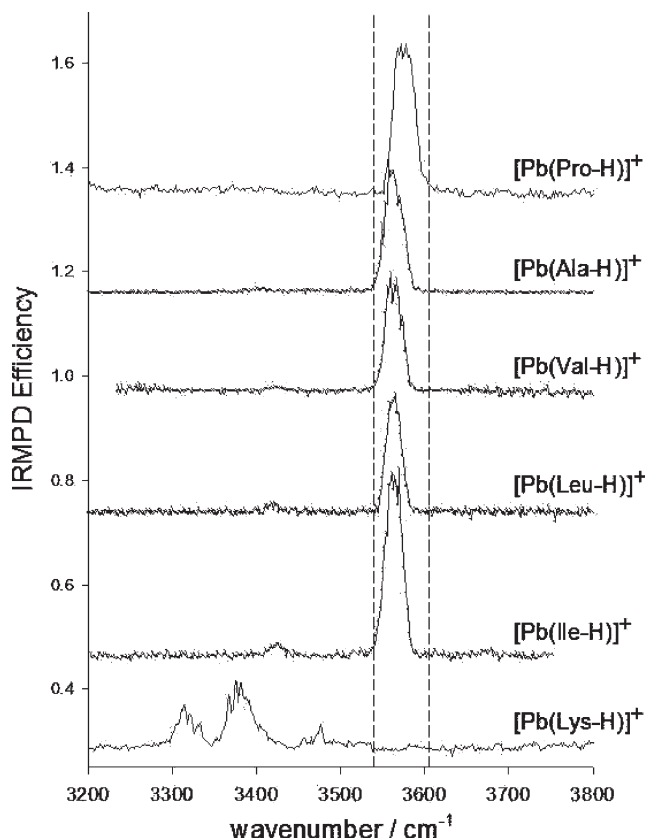


**Figure 2.** IRMPD spectra in the 3200–3800  $\text{cm}^{-1}$  region of the six  $\text{Pb}^{2+}$ /amino acid conjugate base complexes studied in this work.

similar, except that there is nothing observed in the N–H stretch region. This implies that for the  $[\text{Pb}(\text{Aa-H})]^+$  complexes where Aa = Ala, Val, Leu, Ile, and Pro, deprotonation is occurring at the amine moiety and not the carboxylic acid.

The spectrum for  $[\text{Pb}(\text{Lys-H})]^+$  is clearly different than the five complexes discussed above (Figure 2). Most notably, they lack the strong feature at  $\sim 3560 \text{ cm}^{-1}$  assigned to the O–H stretch. This suggests that  $[\text{Pb}(\text{Lys-H})]^+$  is deprotonated at the carboxylic acid end of the amino acid. Furthermore, the IRMPD spectrum of  $[\text{Pb}(\text{Lys-H})]^+$  also contains observable IRMPD efficiency intensity in the N–H stretching region with three main absorptions at 3315, 3380, and 3480  $\text{cm}^{-1}$ .

The  $[\text{Pb}(\text{Aa-H})]^+$  complexes were singly hydrated in the storage hexapole, forming  $[\text{Pb}(\text{Aa-H})\text{H}_2\text{O}]^+$ . The IRMPD spectra of the  $[\text{Pb}(\text{Aa-H})\text{H}_2\text{O}]^+$  complexes are collected in Figure 3. The only fragmentation pathways observed upon irradiation by the KTP OPO were for the loss of  $\text{H}_2\text{O}$ ; however, Ala, Val, Leu, and Ile also showed a much smaller secondary loss of a second  $\text{H}_2\text{O}$  (10% relative to the first loss) over the carboxylic acid O–H stretch region, which is attributed to IRMPD of the  $[\text{Pb}(\text{Aa-H})]^+$  fragment ions. There is a significant difference between the hydrated  $[\text{Pb}(\text{Aa-H})\text{H}_2\text{O}]^+$  complexes containing Ala, Val, Leu, and Ile, and those containing Lys and Pro. The spectra for  $[\text{Pb}(\text{Aa-H})\text{H}_2\text{O}]^+$  (Aa = Ala, Val, Leu, and Ile) each contain weak absorptions due to amine N–H stretching between 3250 and 3400  $\text{cm}^{-1}$  and two much stronger absorptions at 3580 and 3690  $\text{cm}^{-1}$ . These latter two bands are in similar positions to the bands assigned to the carboxylic acid O–H stretch and a  $\text{PbO–H}$  stretch, respectively, for hydrated  $[\text{Pb}(\text{Gly-H})]^+$ .<sup>12</sup>

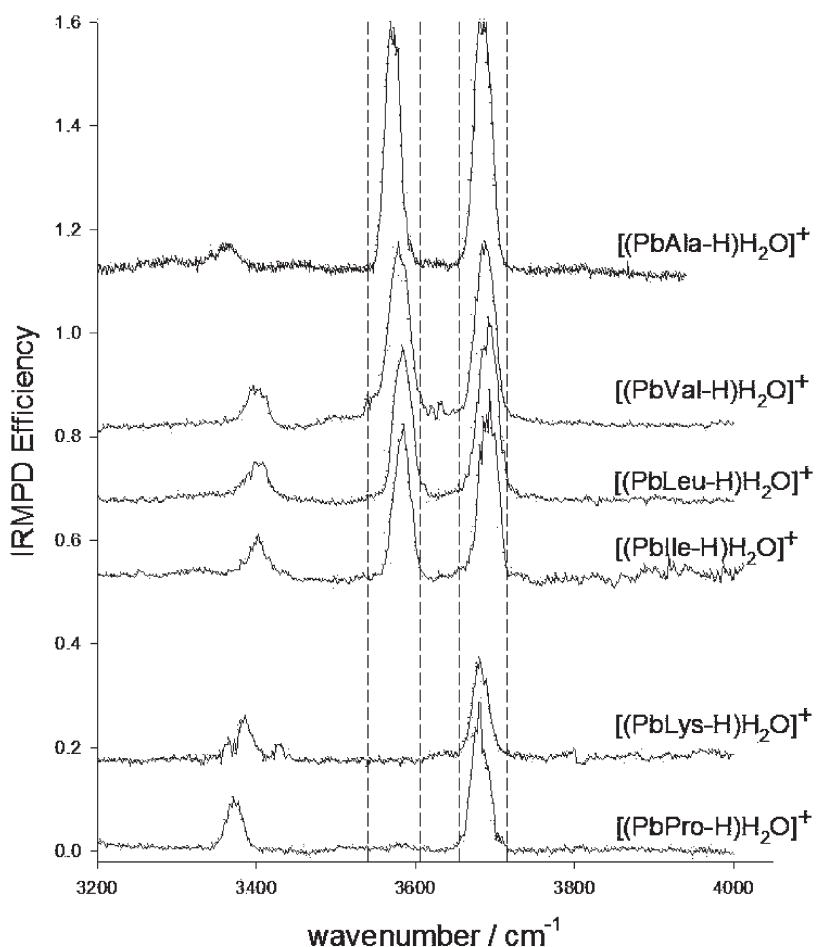


**Figure 3.** IRMPD spectra in the 3200–4000  $\text{cm}^{-1}$  region of the six hydrated  $\text{Pb}^{2+}$ /amino acid conjugate base complexes studied in this work.

The IRMPD spectra of both  $[\text{Pb}(\text{Lys-H})\text{H}_2\text{O}]^+$  and  $[\text{Pb}(\text{Pro-H})\text{H}_2\text{O}]^+$  have only one band in the O–H stretching region at  $\sim 3680 \text{ cm}^{-1}$ . The bare  $[\text{Pb}(\text{Lys-H})]^+$  complex did not have a carboxylic acid O–H stretch. It might be expected that attaching water to  $[\text{Pb}(\text{Lys-H})]^+$  would result in a water symmetric and antisymmetric stretching absorption, but spectroscopically this can be ruled out. Transfer of a proton back to the carboxylate group can also be ruled out based on the absence of this band. A structure where water is coordinated to lead and intramolecularly hydrogen bonded to another basic site in the molecule could explain the spectrum. The spectrum of  $[\text{Pb}(\text{Pro-H})\text{H}_2\text{O}]^+$  is interesting; it does not have a carboxylic acid O–H stretch but the bare complex,  $[\text{Pb}(\text{Pro-H})]^+$ , did. This very likely means that during solvation in the storage hexapole,  $[\text{Pb}(\text{Pro-H})]^+$ , not only solvates but also isomerizes from an amine-deprotonated structure to a carboxylic acid-deprotonated structure.

The structures of these species will now be discussed along with computed IR spectra and relative energies of isomeric structures.

**3.2.  $[\text{Pb}(\text{Ala-H})]^+$  and  $[\text{Pb}(\text{Ala-H})\text{H}_2\text{O}]^+$ .** Figure 4 contains the lowest-energy structures for the  $[\text{Pb}(\text{Ala-H})]^+$  and  $[\text{Pb}(\text{Ala-H})\text{H}_2\text{O}]^+$  complexes. The relative enthalpies and 298 K Gibbs energies, computed using both of the LANL2DZ and SDD methods previously discussed, are also shown. It is evident that the lowest energy structure of  $[\text{Pb}(\text{Ala-H})]^+$ , Ala-A, is N-deprotonated with  $\text{Pb}^{2+}$  bound between  $\text{HN}^-$  and the carbonyl oxygen. Ala-B and Ala-C are both carboxylic acid deprotonated and

significantly higher in energy. Ala-B coordinates  $\text{Pb}^{2+}$  similarly to Ala-A, whereas in Ala-C,  $\text{Pb}^{2+}$  is bound to the carboxylate end. The nearly 90° OCCN dihedral angle for Ala-C is lower in energy than structures with a 0° OCCN angle by 2.5  $\text{kJ mol}^{-1}$ . Also, the computed IR spectra are unaffected by the difference in OCCN dihedral angle in the 3200–3800  $\text{cm}^{-1}$  region of the IR, so only the lowest energy conformers are shown.

When water is added to each of these complexes, the structures depicted on the right-hand side of Figure 4 result. There are two types of structures, where water is intact and where it donates a proton back to where the proton is absent from the nonsolvated complex. For three of the structures where water is intact, AlaW-Ai, AlaW-B, and AlaW-D, proton transfer results in AlaW-Aii. For AlaW-Ci, proton transfer results in AlaW-Cii. Whereas the nonsolvated Ala-C is  $\sim 30 \text{ kJ mol}^{-1}$  higher in Gibbs energy (298 K) than Ala-A, solvating dramatically changes this picture: Solvation of Ala-A produces AlaW-Ai, which is 30.7–40.9  $\text{kJ mol}^{-1}$  higher in Gibbs energy than AlaW-Ci, formed by solvation of Ala-C. The subsequent proton-transfer from water back to N produces roughly isoergonic lowest energy structures; AlaW-Cii is approximately 2.1–4.5  $\text{kJ mol}^{-1}$  lower in Gibbs energy, using MP2 methods, than AlaW-Aii.

The IRMPD spectra of  $[\text{Pb}(\text{Ala-H})]^+$  and  $[\text{Pb}(\text{Ala-H})\text{H}_2\text{O}]^+$  are shown in Figure 5A,B, respectively, along with the B3LYP/6-31+G(d,p) computed IR spectra for the different  $[\text{Pb}(\text{Ala-H})]^+$  and  $[\text{Pb}(\text{Ala-H})\text{H}_2\text{O}]^+$  structures. By comparing the experimental

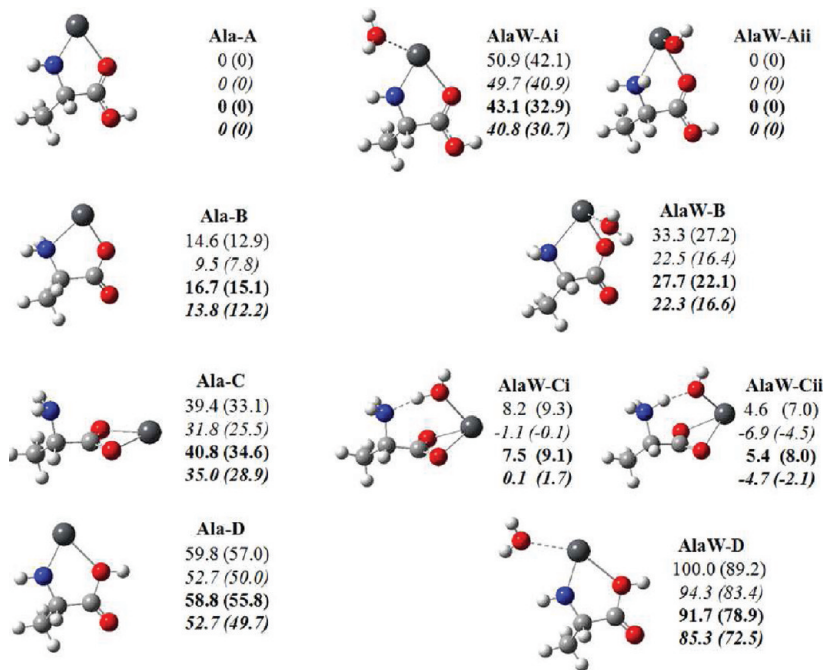


**Figure 4.** B3LYP/6-31+G(d,p) (LANL2DZ on Pb) computed structures for bare and hydrated  $\text{Pb}^{2+}$ /alanine conjugate base complexes. The energies reported are 298 K enthalpies (and Gibbs energies in parentheses). The unbolded values are using the LANL2DZ basis and effective core potential on Pb and the bolded values are using the SDD basis and effective core potential on Pb. The nonitalicized values are B3LYP/6-31+G(d,p) (with LANL2DZ or SDD on Pb) and the italicized values are MP2(full)/6-311++G(2d,2p)//B3LYP/6-31+G(d,p) (with LANL2DZ or SDD on Pb).

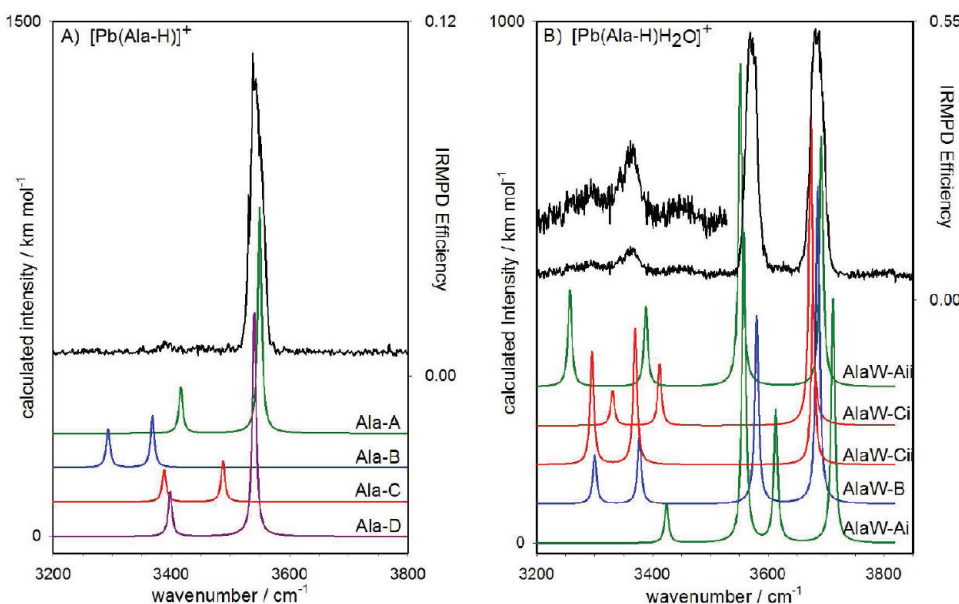


**Figure 5.** Comparison of the IRMPD spectra for the bare (A) and hydrated (B)  $[\text{Pb}(\text{Ala-H})]^+$  complexes with the B3LYP/6-31+G(d,p) calculated spectra for the various isomers displayed in Figure 4.

and computed spectra for  $[\text{Pb}(\text{Ala-H})]^+$ , there is a distinct similarity between the experimental spectrum and the computed spectra for structures Ala-A and Ala-D, and these structures cannot be distinguished simply based on the IRMPD spectrum. Both of these structures are deprotonated at N, but  $\text{Pb}^{2+}$  in Ala-D is bound to the hydroxyl oxygen, rather than the carbonyl as in Ala-A, and is calculated to be  $52.7 \text{ kJ mol}^{-1}$  higher in Gibbs energy. It is, therefore, highly probable that the species

responsible for the experimental spectrum is Ala-A. The strong band at  $3560 \text{ cm}^{-1}$  is assigned to the carboxylic acid O–H stretch, and the weak band at  $3410 \text{ cm}^{-1}$  is the N–H stretch of Ala-A, which is the lowest-energy structure.

The IRMPD spectrum of  $[\text{Pb}(\text{Ala-H})\text{H}_2\text{O}]^+$  is compared with computed spectra for various isomers of  $[\text{Pb}(\text{Ala-H})\text{H}_2\text{O}]^+$  in Figure 5B. The experimental spectrum has only two strong bands in the O–H stretch region. This rules out AlaW-Ai and AlaW-D,

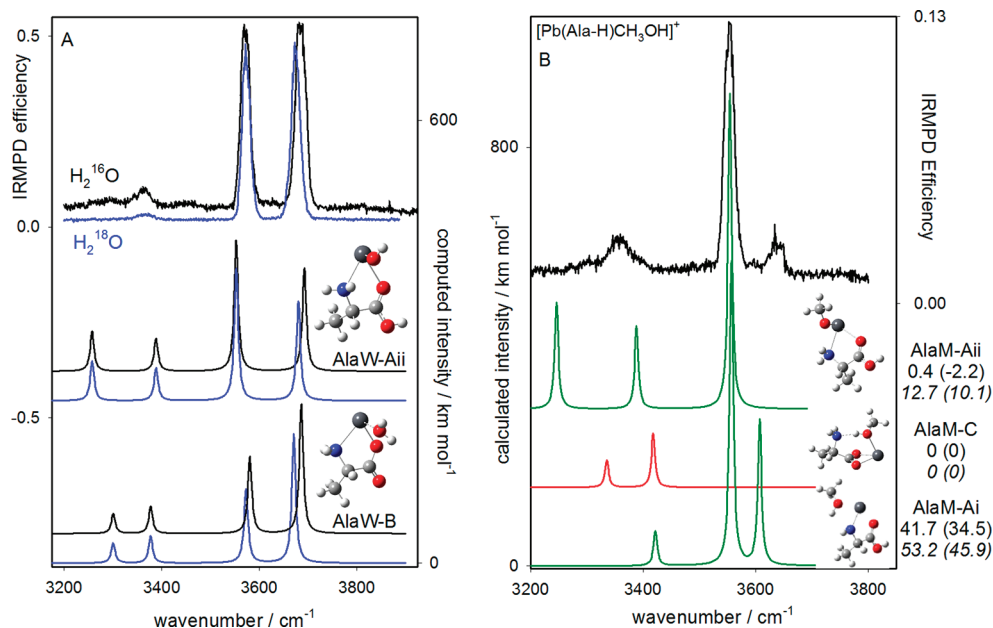


**Figure 6.** (A) Comparison of experimental and computed spectra for  $[\text{Pb}(\text{Ala-H})\text{H}_2^{16}\text{O}]^+$  and  $[\text{Pb}(\text{Ala-H})\text{H}_2^{18}\text{O}]^+$ . (B) Comparison of the experimental IRMPD spectrum for  $[\text{Pb}(\text{Ala-H})\text{CH}_3\text{OH}]^+$  and the computed spectra for three of the isomeric structures. 298 K enthalpies (and Gibbs energies in parentheses) displayed are computed using B3LYP/6-31+G(d,p) (nonitalicized, with LANL2DZ on Pb) and MP2(full)/6-311+G(2d,2p)//B3LYP/6-31+G(d,p) (italicized, with LANL2DZ on Pb).

the complexes formed simply by adding water to Ala-A and Ala-D, respectively, which are expected to both have a water antisymmetric and symmetric stretch as well as the carboxylic acid O–H stretch. Structures AlaW-Aii and AlaW-B both compare very well with the experimental spectrum. In the first case, AlaW-Aii, this suggests that water has transferred a proton back to the deprotonated site on the amino acid, leaving a PbO–H stretch observed at  $3690\text{ cm}^{-1}$  and a carboxylic acid O–H stretch at  $3580\text{ cm}^{-1}$ . AlaW-B could be formed by simply adding water to Ala-B. AlaW-B is significantly higher in energy than AlaW-Aii, but it is possible to experimentally rule out AlaW-B as a contributor to the IRMPD spectrum by adding oxygen-18-labeled water to the electrosprayed complex in the hexapole cell. If both bands observed were due to water stretches, then both bands would be expected to shift. If the  $3680\text{ cm}^{-1}$  band was due to the carboxylic acid O–H stretch, then that band would not shift upon the addition of oxygen-18-labeled water. The experimental spectra when normal water and oxygen-18-labeled water were added to  $[\text{Pb}(\text{Ala-H})]^+$  are shown in Figure 6A in black and blue, respectively. The predicted spectra for AlaW-Aii and AlaW-B, with both normal and oxygen-18-labeled water added to Pb, are also shown. The absence of a shift in the  $3580\text{ cm}^{-1}$  and a shift in the  $3690\text{ cm}^{-1}$  band confirms the absence of AlaW-B and, in fact, any structure where there is free water bound to the  $[\text{Pb}(\text{Ala-H})]^+$  complex.

AlaW-Ci and AlaW-Cii are computed to be similar in energy to AlaW-Aii but are expected to have only one band in the O–H stretch region. Whereas the presence of the  $3680\text{ cm}^{-1}$  band does confirm the presence of a structure such as AlaW-Aii, it does not necessarily rule out the presence of AlaW-Ci and AlaW-Cii. In fact, the N–H stretch region is more complex than the two N–H stretching vibrations of AlaW-Aii would suggest; there is observable IRMPD intensity at  $\sim 3450\text{ cm}^{-1}$  between the carboxylic acid O–H stretch and the most intense N–H

stretching vibration (observed at  $3370\text{ cm}^{-1}$ ) that might be consistent with one or both of the AlaW-C isomers being present as well as AlaW-Aii. Similarly, the band observed at the lowest frequency is broad and may be so because of it being composed of more than one vibration, although it could also be that in AlaW-Aii the N–H bond has a small degree of interaction with the oxygen of the PbOH moiety. On the basis of the present data, it is difficult to rule out the AlaW-C structures, but it is quite apparent from the intense carboxylic acid O–H stretch observed that there is a significant contribution from AlaW-Aii. If the AlaW-C structures are present, then it likely means that during the solvation of AlaW-A in the hexapole storage cell there is also isomerization occurring.

An IRMPD spectrum was also recorded for  $[\text{Pb}(\text{Ala-H})]^+$  solvated by methanol,  $[\text{Pb}(\text{Ala-H})\text{CH}_3\text{OH}]^+$ . The spectrum shown in Figure 6B exhibits IRMPD intensity in the N–H stretch region and, similar to the  $[\text{Pb}(\text{Ala-H})]^+$  and  $[\text{Pb}(\text{Ala-H})\text{-H}_2\text{O}]^+$  spectra, a strong band at  $\sim 3560\text{ cm}^{-1}$  consistent with a carboxylic acid O–H stretch. There is also a weaker band at  $3640\text{ cm}^{-1}$ . If we were observing a structure similar to AlaW-Aii for  $[\text{Pb}(\text{Ala-H})\text{H}_2\text{O}]^+$ , then we would not expect to see a band in this region because the PbOH moiety is changed to PbOCH<sub>3</sub> with methanol as the solvent. Solvating Ala-C would not exhibit the carboxylic acid O–H stretch and, unless the hydrogen bonding similar to that observed for the AlaW-C structures was absent, there would not be a methanol free O–H stretch. In Figure 6B, the experimental IRMPD spectrum is compared with three structures AlaM-Ai, AlaM-Aii, and AlaM-C. It is apparent that we cannot rule out any of these structures. In fact, even AlaM-Ai, which is predicted to be  $34.5\text{ kJ mol}^{-1}$  higher in Gibbs energy than AlaM-Aii, cannot be ruled out. AlaM-Ai is most likely responsible for the  $3640\text{ cm}^{-1}$  band. This is the entrance channel complex between methanol and Ala-A,

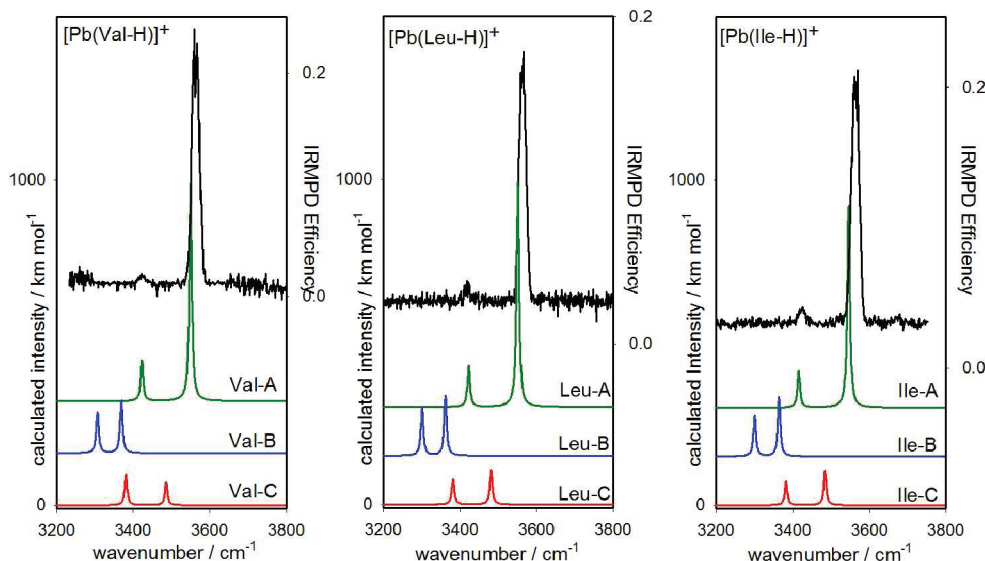


**Figure 7.** IRMPD spectra of the bare complexes between  $\text{Pb}^{2+}$  and the conjugate bases of Val, Leu, and Ile compared with the B3LYP/6-31+G(d,p) computed spectra for the A-, B-, and C-type structures seen in Figure 8.

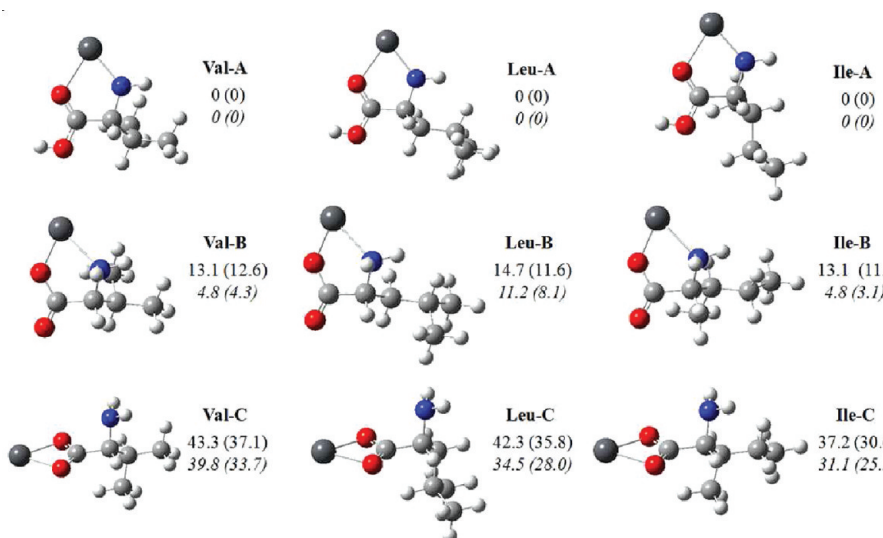


**Figure 8.** Computed structures for the complexes between  $\text{Pb}^{2+}$  and the conjugate bases of Val, Leu, and Ile. 298 K enthalpies (and Gibbs energies in parentheses) displayed are computed using B3LYP/6-31+G(d,p) (nonitalicized, with LANL2DZ on Pb) and MP2(full)/6-311++G(2d,2p)//B3LYP/6-31+G(d,p) (italicized, with LANL2DZ on Pb).

and its presence suggests that some of this complex gets kinetically trapped in this structure and proton transfer to N is not complete.

**3.3.  $[\text{Pb}(\text{Val-H})]^+$ ,  $[\text{Pb}(\text{Leu-H})]^+$ ,  $[\text{Pb}(\text{Ile-H})]^+$  and their Monohydrated Analogues.** The IRMPD spectra of the bare  $[\text{Pb}(\text{Val-H})]^+$ ,  $[\text{Pb}(\text{Leu-H})]^+$ , and  $[\text{Pb}(\text{Ile-H})]^+$  complexes are compared with computed IR spectra in Figure 7. The three lowest-energy structures for each of these complexes are shown in Figure 8. These spectra are very similar to the spectrum of  $[\text{Pb}(\text{Ala-H})]^+$  in Figure 5. It is clear, by comparing the computed and experimental spectra, that the main contributor to each spectrum is the lowest energy isomer (Val-A, Leu-A, and Ile-A) in each case.

In Figure 9 are the IRMPD spectra for the monohydrated species,  $[\text{Pb}(\text{Val-H})\text{H}_2\text{O}]^+$ ,  $[\text{Pb}(\text{Leu-H})\text{H}_2\text{O}]^+$ , and  $[\text{Pb}(\text{Ile-H})\text{H}_2\text{O}]^+$ .

$\text{H}_2\text{O}]^+$ . Also, in Figure 9, and compared with the experimental spectra, are the computed spectra for the lowest-energy hydrated structures for each of the three bare clusters. The computed structures and relative energies for the lowest energy hydrated complexes are shown in Figure 10. The B3LYP calculated energies predict the A and C structures to be similar in energy. The MP2 calculations predict the C structures, being deprotonated at the carboxylic acid and with lead bound to the carboxylate, to be lower in Gibbs energy than the A structures by between 4.6 and 13.9  $\text{kJ mol}^{-1}$ . However, our experimental spectra clearly show that the main structures contributing to the spectra are the A structures. As it was for the  $[\text{Pb}(\text{Ala-H})\text{H}_2\text{O}]^+$ , the B structures can be ruled out by isotopic labeling experiments that show only a shift in the  $\text{PbO-H}$  stretching vibration, as seen for  $[\text{Pb}(\text{Val-H})\text{H}_2\text{O}]^+$ . The calculations also show the

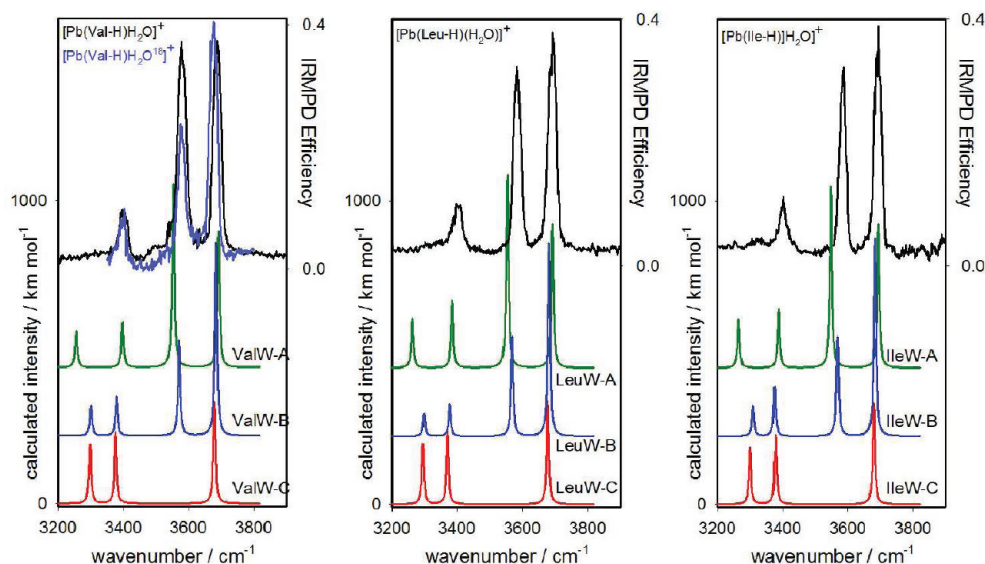


**Figure 9.** IRMPD spectra of the singly hydrated complexes between  $\text{Pb}^{2+}$  and the conjugate bases of Val, Leu, and Ile compared with the B3LYP/6-31+G(d,p) computed spectra for the A-, B-, and C-type structures seen in Figure 10.

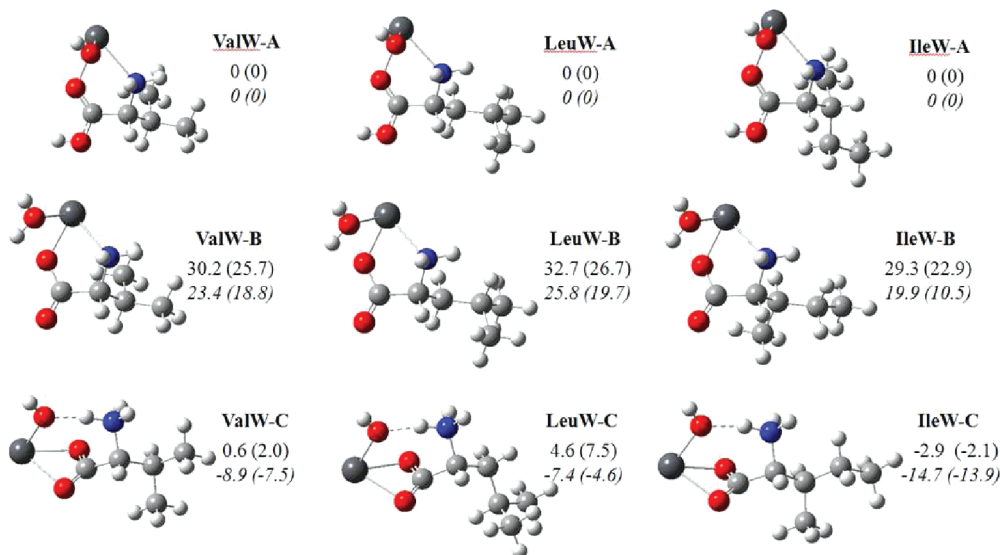


**Figure 10.** Computed structures for the hydrated complexes between  $\text{Pb}^{2+}$  and conjugate bases of either Val, Leu, or Ile. 298 K enthalpies (and Gibbs energies in parentheses) displayed are computed using B3LYP/6-31+G(d,p) (nonitalicized, with LANL2DZ on Pb) and MP2(full)/6-311+G(2d,2p)//B3LYP/6-31+G(d,p) (italicized, with LANL2DZ on Pb).

B structures to be significantly higher in energy. For the nonhydrated species, the A structures were computed to be the lowest in Gibbs energy over the C structures by at least 25.3  $\text{kJ mol}^{-1}$ , and the spectra are consistent with the A structures. The fact that the A structures seem to be the main species present in the hydrated system suggests that the A structures are solvated, and the energy barrier for isomerization to the hydrated C structures is too high to be overcome on the time scale of the present experiments or that the calculations artificially stabilize the C structures with respect to the A structures. We will have a little more to say about this in the next section.

**3.4.  $[\text{Pb}(\text{Pro-H})]^+$  and  $[\text{Pb}(\text{Pro-H})\text{H}_2\text{O}]^+$ .** The spectrum of  $[\text{Pb}(\text{Pro-H})]^+$  is compared with the computed spectra for

the three lowest energy isomers (structures in Figure 12) in Figure 11. Clearly, there is a carboxylic acid O—H stretch and no observable N—H stretch, suggesting that proline is, like the other systems discussed so far, amine-deprotonated. The calculations predict that Pro-B is actually lower in Gibbs energy than Pro-A by 11.5  $\text{kJ mol}^{-1}$  using MP2 theory and the LANL2DZ basis and core potential on Pb. Calculations employing the SDD basis and core potential yield slightly different results in that the two isomers are virtually identical in energy. Our experimental spectrum, however, is most consistent with Pro-A. The fact that simply changing a basis set produces different minimum energy structures demonstrates the importance that experiments have in revealing structural information. One cannot solely rely on calculations.

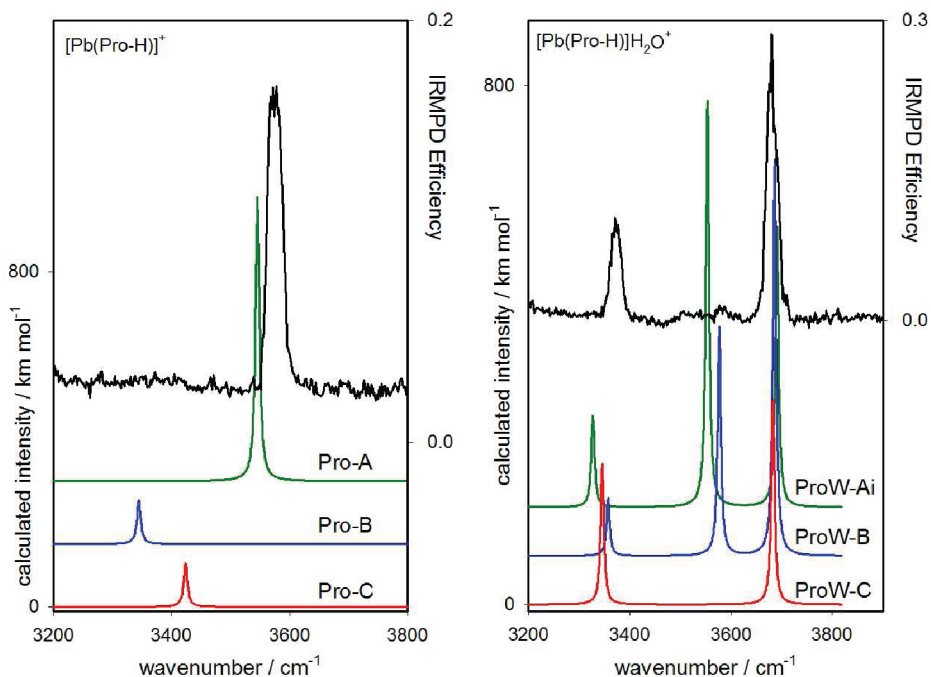


**Figure 11.** Comparison of the IRMPD spectra of the bare and hydrated complexes between  $\text{Pb}^{2+}$  and conjugate base of Pro and the computed structures shown in Figure 12.

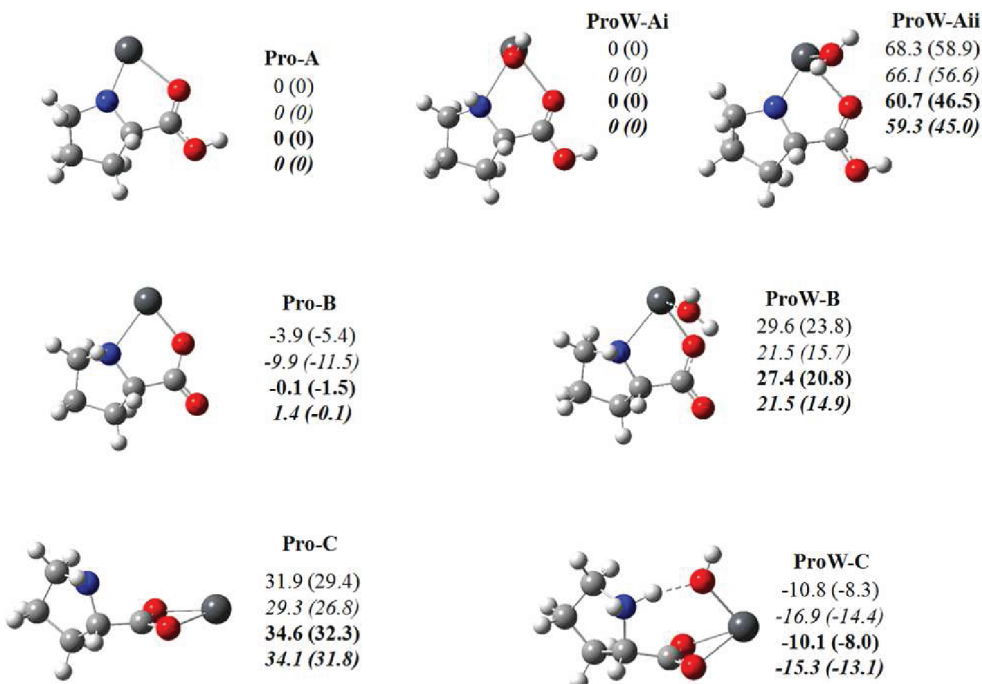


**Figure 12.** B3LYP/6-31+G(d,p) (LANL2DZ on Pb) computed structures for bare and hydrated  $\text{Pb}^{2+}$ /proline conjugate base complexes. The energies reported are 298 K enthalpies (and Gibbs energies in parentheses). The unbolted values are using the LANL2DZ basis and effective core potential on Pb and the bolded values are using the SDD basis and effective core potential on Pb. The nonitalicized values are B3LYP/6-31+G(d,p) (with LANL2DZ or SDD on Pb) and the italicized values are MP2(full)/6-311++G(2d,2p)//B3LYP/6-31+G(d,p) (with LANL2DZ or SDD on Pb).

The IRMPD spectrum of  $[\text{Pb}(\text{Pro-H})\text{H}_2\text{O}]^+$  (Figures 2 and 11) is markedly different from the amino acid complexes discussed above. The strong carboxylic acid O–H stretch band between 3560 and  $3580 \text{ cm}^{-1}$  observed in the bare and hydrated  $[\text{Pb}(\text{Ala-H})]^+$ ,  $[\text{Pb}(\text{Val-H})]^+$ ,  $[\text{Pb}(\text{Leu-H})]^+$ , and  $[\text{Pb}(\text{Ile-H})]^+$  complexes and in

$[\text{Pb}(\text{Pro-H})]^+$  is absent. In Figure 11, computed spectra are compared with the experimental spectra for  $[\text{Pb}(\text{Pro-H})\text{H}_2\text{O}]^+$ . It is clear that because of the absence of the band in the 3560 and  $3580 \text{ cm}^{-1}$  region ProW-Ai and ProW-B cannot explain the observed spectrum. ProW-C is computed to be lower in 298 K

Gibbs energy than ProW-Ai by approximately 14.4 or 13.1 kJ mol<sup>-1</sup>, depending on whether LANL2DZ or the SDD basis set and ECP, respectively, was used for lead.

These experiments show that when hydrated, or during the hydration process, electrosprayed Pro-A, observed in the IRMPD experiments, isomerizes to Pro-C so that the hydrated isomer observed is ProW-C. The question is why does this same process not happen for Ala-A, Val-A, Leu-A, and Ile-A, all of which are observed in the IRMPD experiments, as are the hydrated A isomers, AlaW-A, ValW-A, LeuW-A, and IleW-A? To answer this question, we computed the potential energy surface for isomerization of Ala-A to Ala-C and for Pro-A to Pro-C (Figures S1 and S2 of the Supporting Information, respectively). For both systems, the path from the A to the C isomers goes through the D and then the B isomers. The main Gibbs energy barrier for these isomerizations would be two hydrogen transfer reactions, the highest being isomerization of the D isomers to the B isomers, a transfer of a proton from O—H to N that requires 207 and 223 kJ mol<sup>-1</sup> for the Ala and Pro systems, respectively. These energy barriers are far too high for these reactions to take place in the gas phase, and there is no thermodynamic grounds for isomerization because both rearrangements are an uphill processes requiring some 30 kJ mol<sup>-1</sup>.

As previously stated, in both instances, the bare complexes observed were the A isomers, Ala-A and Pro-A. It is the hydrated isomeric structures that differ. A likely place for isomerization to occur is in the storage hexapole, which has a modest pressure of water vapor,  $\sim 10^{-2}$  mbar. One could envisage that after the first addition of water, a second water could assist in any proton transfer isomerizations. A direct, second water-assisted isomerization for the A isomers directly to the B isomers was found with a barrier of only just above 30 kJ mol<sup>-1</sup>, as seen in Figure 13A,B for alanine and proline, respectively. The second step in both cases is a change in lead binding from N and O to the two carboxylate oxygens, this complex being the global minimum on the  $[\text{Pb}(\text{Aa-H})\text{H}_2\text{O}]^+$  surface. This final isomerization is not assisted by water and has a Gibbs energy barrier of 175 kJ mol<sup>-1</sup> for the Ala case but only 98 kJ mol<sup>-1</sup> for the Pro system (the MP2 Gibbs energy barriers are 166 and 82 kJ mol<sup>-1</sup>, respectively), as seen in Figure 13A,B. Whereas there is very likely some uncertainty in the magnitudes of these Gibbs energy barriers, the relative barriers are probably trustworthy. It is clear that for AlaW-B to AlaW-C isomerization the rate constant will be orders of magnitude smaller than those for the ProW-B to ProW-C isomerization, in fact  $10^{14}$  times slower based on the MP2 Gibbs energies at 298 K. This would account for why isomerization occurs in the Pro system and ProW-C is observed in the IRMPD spectrum but in the Ala system isomerization does not occur and the main isomer observed in the IRMPD spectrum is ProW-Aii.

This very large difference in the Gibbs energy barriers also brings up the question as to the source of this difference. Being a secondary amine, proline is significantly more basic than alanine; the gas basicity of proline is 928 kJ mol<sup>-1</sup>, versus 888 kJ mol<sup>-1</sup> for alanine.<sup>67</sup> One of the reasons is the main transition state for proline is better stabilized by a much stronger water O—H $\cdots$ N hydrogen bond, 1.952 Å, in the proline transition state versus 2.020 Å for the alanine transition state (Figure 13A,B). The greater basicity also results in a slightly longer N—Pb bond for the transition state in Pro so that the transition state is more product-like and less tight. The fact that proline is more basic than all of alanine, valine, leucine, and isoleucine and is better at stabilizing the transition state from N and O bound Pb to

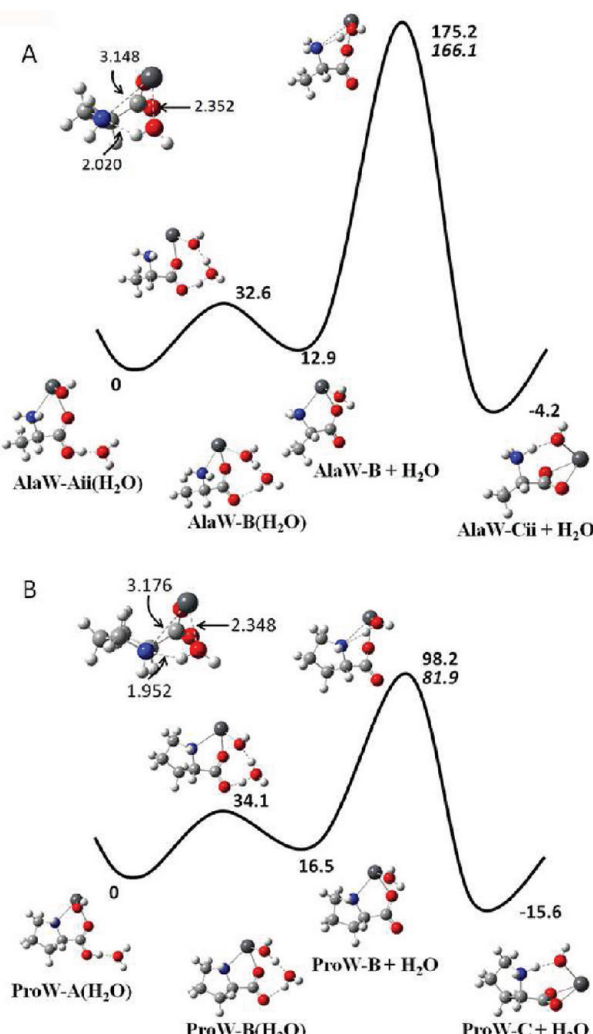


**Figure 13.** 298 K Gibbs energy diagram for the isomerization of the hydrated A-type structures to the hydrated C-type structures for alanine (A) and proline (B). Note that the first isomerization is water assisted or catalyzed.

carboxylate-bound Pb could explain why isomerization is observed to occur in the proline case but not for any of the others.

**3.5.  $[\text{Pb}(\text{Lys-H})]^+$  and  $[\text{Pb}(\text{Lys-H})\text{H}_2\text{O}]^+$ .** The side chain of lysine is basic and can interact with the lead cation. The lowest energy structures are displayed in Figure 14. It is evident by comparing the structures where the side chain is interacting with lead (Lys-A, -B, and -C) with those where the side chain is not interacting with lead that  $\text{Pb}^{2+}$  (Lys-Ai, -Bi, and -Ci) is greatly stabilized by an interaction with the amine group of the lysine side chain. Without any interaction with the side chain, the Ai, Bi, and Ci structures are similar in relative energy to the previously discussed systems with Ai and Bi being of similar thermodynamic stability and the Ci structure being higher in Gibbs energy by 29.6–31.7 kJ mol<sup>-1</sup>. The Bi and Ci structures, deprotonated at the carboxylic acid, are stabilized by an interaction between the side chains and lead to a much greater extent (96.6 and 127.0 kJ mol<sup>-1</sup>, respectively) than the Ai structure (59.9 kJ mol<sup>-1</sup>), which is deprotonated at the amine group. This extra stabilization of the lead ion by the side chain renders the Lys-C structure

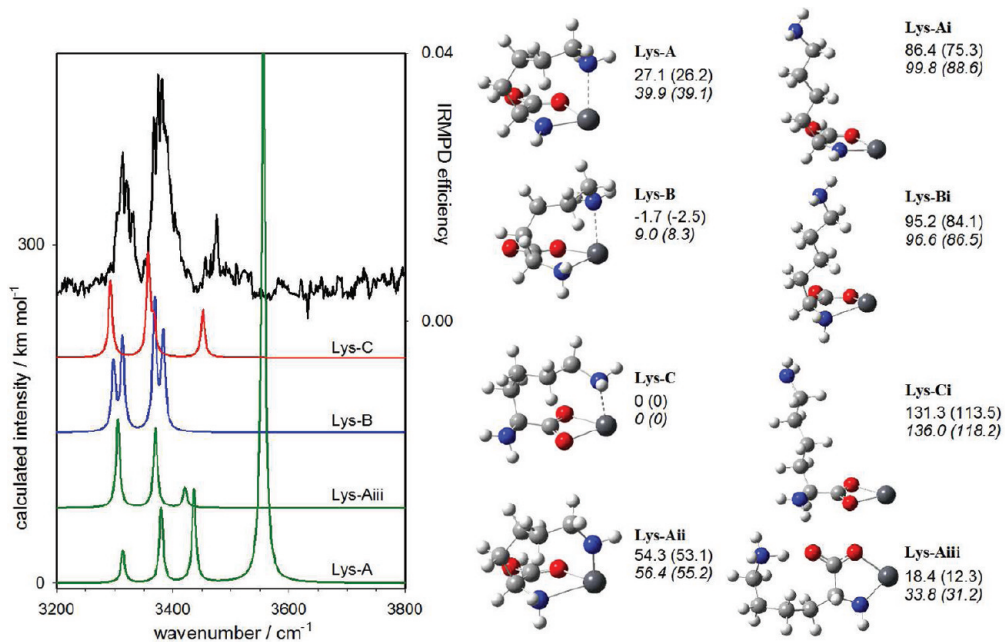


**Figure 14.** Comparison of the IRMPD spectra of the bare complexes between  $\text{Pb}^{2+}$  and conjugate base of Lys and the computed spectra for some of the B3LYP/6-31+G(d,p) (LANL2DZ on Pb) computed structures shown. 298 K enthalpies (and Gibbs energies in parentheses) displayed are computed using B3LYP/6-31+G(d,p) (nonitalicized, with LANL2DZ on Pb) and MP2(full)/6-311++G(2d,2p)//B3LYP/6-31+G(d,p) (italicized, with LANL2DZ on Pb).

significantly lower in energy than the Lys-A structure, in contrast with systems discussed in the previous sections. The structure where deprotonation occurs at the amine side chain, Lys-Aii, is shown for comparison in Figure 14 and is significantly higher in energy. A third A-type structure (Lys-Aiii), where the carboxylic acid OH is hydrogen-bonded to the side-chain amine group was optimized, and, in fact, the proton transferred from the carboxylic acid group to the side chain in a zwitterionic structure. The resulting  $-\text{NH}_3^+$  is hydrogen-bonded to the  $-\text{COO}^-$  group. The Gibbs energy of this structure is actually slightly lower ( $\sim 8 \text{ kJ mol}^{-1}$ ) than Lys-A but is still some  $30 \text{ kJ mol}^{-1}$  higher in energy than the lowest energy structure, Lys-C.

The IRMPD spectrum of  $[\text{Pb}(\text{Lys-H})]^+$  is also shown in Figure 14 with the computed IR spectra of the four lowest energy  $[\text{Pb}(\text{Lys-H})]^+$  structures. The experimental spectrum exhibits three main features at 3360, 3390, and 3430 cm<sup>-1</sup>, in the N–H stretching region. Unlike the spectra of the bare  $[\text{Pb}(\text{Aa-H})]^+$  ions discussed in previous sections, there is no carboxylic acid O–H stretch that rules out the structures where deprotonation occurs at the amine group except for Lys-Aiii, which is also deprotonated at the carboxylic acid group. This is consistent with these structures (Lys-A and Lys-Aii) being computed to be significantly higher in energy. The structure with the computed spectrum that is most consistent with the experimental spectrum is Lys-C, which is also the one that is predicted to be the lowest in enthalpy and Gibbs energy at the MP2 level of theory. Whereas experimentally, Lys-C and Lys-Aii cannot be ruled out as contributing to the IR spectrum, the computed Gibbs energy predicts it to be a quite minor component.

Figure 15 shows seven of the lowest energy structures for  $[\text{Pb}(\text{Lys-H})\text{H}_2\text{O}]^+$ . The lowest energy structure, unlike the bare complex, is a three-coordinate B-type complex, but instead of the side chain interacting with lead, lead is hydroxylated and a proton

has been transferred to the side chain, which is hydrogen-bonded to both the PbOH and the carboxylic acid hydroxyl group. The B structure where water is intact (LysW-Bii) is  $51.1 \text{ kJ mol}^{-1}$  higher in Gibbs energy than LysW-Bi. In LysW-Bii, the side chain is coordinated to lead. The C structures are predicted to be slightly higher in energy than the B structure. LysW-Cii with water intact is, again, four-coordinate but is only predicted to be  $5.7 \text{ kJ mol}^{-1}$  higher in Gibbs energy than LysW-Ci. LysW-Ai and LysW-Aii are  $35.1$  and  $70.0 \text{ kJ mol}^{-1}$  higher in Gibbs energy than LysW-Bi. The lowest-energy zwitterionic structure, LysW-Aiii (similar to Lys-Aiii in Figure 14), is also significantly higher in energy than the lowest energy structure.

The experimental spectrum is also compared with the computed spectra for the three lowest energy structures in Figure 15. Any of the complexes with intact water will obviously not agree with experimental spectra because there would be two bands in the OH stretch region as for LysW-Cii. Similarly, LysW-Ai cannot reproduce the experimental spectrum because there would be a carboxylic acid O–H stretch as well as the PbO–H stretch. LysW-Bi is the most consistent with the experimental spectrum and actually reproduces it quite well. It is also the lowest energy structure. There are three N–H stretches observed that are consistent with this structure as two of the N–H bonds are hydrogen bonded and predicted to occur at much lower frequencies, out of the range of our experiments. There is no experimental or theoretical evidence for any of the other structures contributing to the spectrum. A B-type structure for the solvated  $[\text{Pb}(\text{Lys-H})]^+$  complex and a C-type structure for the bare complex means that during solvation an isomerization reaction occurs where lead is transferred from the N and O binding to COO<sup>-</sup> binding, similar to the proline complexes. A determination of the potential energy surface for this isomerization is beyond the scope of this work.

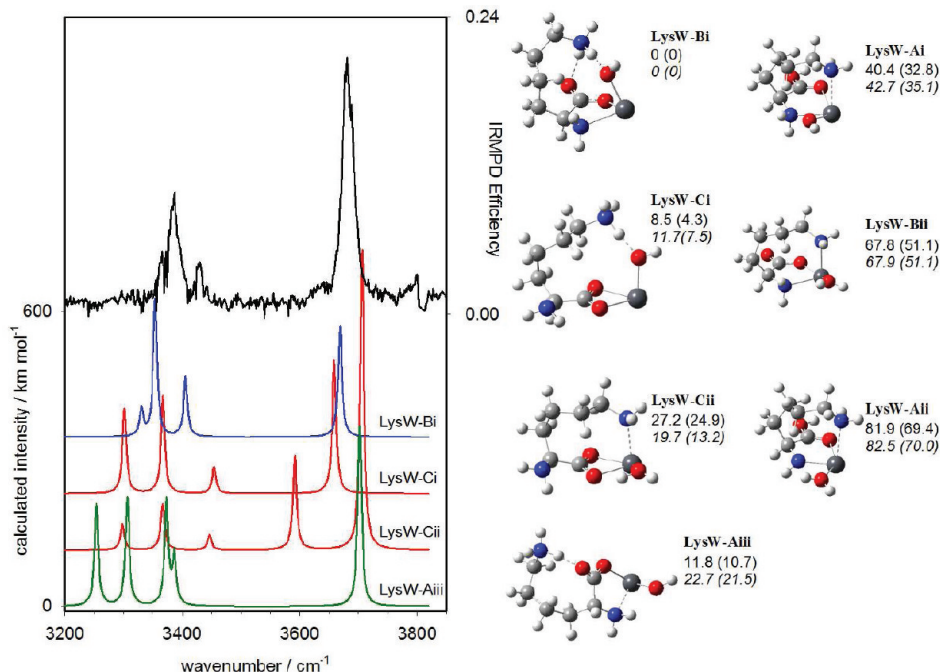


**Figure 15.** Comparison of the IRMPD spectra of the hydrated complexes between  $\text{Pb}^{2+}$  and conjugate base of Lys and the computed spectra for some of the B3LYP/6-31+G(d,p) (LANL2DZ on Pb) computed structures shown. 298 K enthalpies (and Gibbs energies in parentheses) displayed are computed using B3LYP/6-31+G(d,p) (nonitalicized, with LANL2DZ on Pb) and MP2(full)/6-311++G(2d,2p)//B3LYP/6-31+G(d,p) (italicized, with LANL2DZ Pb).

#### 4. CONCLUSIONS: $\text{Pb}^{2+}$ STABILIZATION BY AMINO ACID CONJUGATE BASES

IRMPD spectroscopy and electronic structure calculations both confirmed that  $[\text{Pb}(\text{Aa-H})]^+$  complexes are deprotonated at the amine group (A-type structures) for amino acids with a nonpolar side chain or when the side chain is not interacting with lead.  $\text{Pb}^{2+}$  is typically considered to be a soft (or intermediate) Lewis acid and prefers to bond covalently to soft bases. The carboxylate anion is a hard base, whereas the  $\text{NH}_2$ ,  $\text{NH}$ ,  $\text{NH}\Gamma$ , or  $\text{N}\Gamma$  group would all be considered to be much softer, which accounts for the preferred binding by lead. The fact that the A-type structures are preferred means that there is extra stabilization of  $\text{Pb}^{2+}$  by the  $\text{NH}\Gamma$  or  $\text{N}\Gamma$  group over the  $\text{NH}_2$  or  $\text{NH}$  that overcomes the relatively higher energy of deprotonating the amine group compared with the carboxylic acid. The extra stabilization of  $\text{Pb}^{2+}$  by lysine's basic side chain makes the C-type structure, deprotonated at the carboxylic acid, more stable than the amine deprotonated A-type structure.

When the complex is hydrated, the calculations predict that the C-type structures are the lowest in energy due to the stabilization of  $\text{Pb}^{2+}$  by the extra coordination of water and the hydrogen bonding between the protonated amine and the O of the  $\text{PbOH}$  moiety. However, our experimental IRMPD spectra are most consistent with the A-type structures having an intact carboxylic acid when the amino acid is Ala, Val, Leu, and Ile. These conclusions are supported by experiments with isotopically labeled water where the  $\text{PbO-H}$  stretch was observed to shift upon isotopic substitution but the carboxylic acid O–H stretch did not shift. This is explained by the presence of an insurmountable barrier for isomerization of the A-type hydrated structure to the C-type hydrated structure in the hexapole storage cell, where A-type ions are hydrated. For the bare proline complex, the amine-deprotonated A-type structure is observed, but for

the hydrated complex, the C-type structure is observed. This means that proline isomerization must occur during hydration. A mechanism for isomerization of the A-type structure to the C-type structure, part of which is a base (water)-catalyzed proton transfer isomerization, was determined and is consistent with a much larger barrier ( $>80 \text{ kJ mol}^{-1}$ ) for isomerization in the case of Ala than when Pro is the amino acid. This lower barrier is explained in terms of the greater basicity of proline, which stabilizes lead in the transition state. Experiment and theory also show that the lowest energy structure of  $[\text{Pb}(\text{Lys-H})\text{H}_2\text{O}]^+$  is the B-type structure, deprotonated at the carboxylic acid. In this case, the basic side chain provides the extra stability.

#### ■ ASSOCIATED CONTENT

**S Supporting Information.** Potential energy surfaces for the rearrangements of the A-type amine-deprotonated  $[\text{Pb}(\text{Ala-H})]^+$  and  $[\text{Pb}(\text{Pro-H})]^+$  to their carboxyl-deprotonated C-type isomers. This material is available free of charge via the Internet at <http://pubs.acs.org>.

#### ■ ACKNOWLEDGMENT

We gratefully acknowledge NSERC and CFI for funding and would also like to thank Westgrid and ACENet for computational resources. M.B.B. also thanks NSERC for a Canadian Graduate Scholarship.

#### ■ REFERENCES

- (1) Hajieva, P.; Behl, C. *Curr. Pharm. Des.* **2006**, *12*, 699–704.
- (2) Velez, S.; Nair, N. G.; Reddy, P. *Colloids Surf, B* **2008**, *291*–294.
- (3) Fisher, A. E. O.; Naughton, D. P. *P. J. Struct. Chem.* **2006**, *47*, 87–90.

- (4) Fisher, A. E. O.; Naughton, D. P. *J. Struct. Chem.* **2007**, *48*, 711–714.
- (5) Fisher, A. E. O.; Naughton, D. P. *Biomed. Pharmacother.* **2005**, *59*, 158–162.
- (6) Burford, N.; Eelman, M. D.; LeBlanc, W. G. *Can. J. Chem.* **2004**, *82*, 1254.
- (7) Burford, N.; Eelman, M. D.; LeBlanc, W. G.; Cameron, S.; Robertson, K. N. *Chem. Commun.* **2004**, 332.
- (8) Burford, N.; Eelman, M. D.; Groom, K. J. *Inorg. Chem.* **2005**, *99*, 1992–1997.
- (9) Fridgen, T. D. *Mass Spectrom. Rev.* **2009**, *28*, 586.
- (10) Eyler, J. R. *Mass Spectrom. Rev.* **2009**, *28*, 448.
- (11) Polfer, N. C.; Oomens, J. *Mass Spectrom. Rev.* **2009**, *28*, 468.
- (12) Atkins, C. G.; Banu, L.; Rowsell, M.; Blagojevic, V.; Bohme, D. K.; Fridgen, T. D. *J. Phys. Chem. B* **2009**, *113*, 14457–14464.
- (13) Atkins, C. G.; Rajabi, K.; Gillis, E. A. L.; Fridgen, T. D. *J. Phys. Chem. A* **2008**, *112*, 10220–10225.
- (14) Cagmat, E. B.; Szczepanski, J.; Pearson, W. L.; Powell, D. H.; Eyler, J. R.; Polfer, N. C. *Phys. Chem. Chem. Phys.* **2010**, *12*, 3474–3479.
- (15) Bush, M. F.; O'Brien, J. T.; Prell, J. S.; Wu, C.-C.; Saykally, R. J.; Williams, E. R. *J. Am. Chem. Soc.* **2009**, *131*, 13270–13277.
- (16) Bush, M. F.; O'Brien, J. T.; Prell, J. S.; Saykally, R. J.; Williams, E. R. *J. Am. Chem. Soc.* **2007**, *129*, 1612–1622.
- (17) Oh, H.; Breuker, K.; Sze, S. K.; Ge, Y.; Carpenter, B. K.; McLafferty, F. W. *Proc. Natl. Acad. Sci. U.S.A.* **2002**, *99*, 15863.
- (18) Oepts, D.; van der Meer, A. F. G.; van Amersfoort, P. W. *Infrared Phys. Technol.* **1995**, *36*, 297.
- (19) Ortega, J. M.; Berset, J. M.; Chaput, R.; Glotin, F.; Humbert, G.; Jaroszynski, D.; Joly, P.; Kergosien, B.; Lesrel, J. *Nucl. Instrum. Methods Phys. Res., Sect. A* **1996**, *375*, 618.
- (20) Kamariotis, A.; Boyarkin, O. V.; Mercier, S. R.; Beck, R. D.; Bush, M. F.; Williams, E. R.; Rizzo, T. R. *J. Am. Chem. Soc.* **2006**, *128*, 905–916.
- (21) Locke, M. J.; McIver, R. T. *J. Am. Chem. Soc.* **1983**, *105*, 4226–4232.
- (22) Chapo, C. J.; Paul, J. B.; Provencal, R. A.; Roth, K.; Saykally, R. J. *J. Am. Chem. Soc.* **1998**, *120*, 12956–12957.
- (23) Bachrach, S. M.; Nguyen, T. T.; Demoin, D. W. *J. Phys. Chem. A* **2009**, *113*, 6172–6181.
- (24) Ahn, D.-S.; Park, S.-W.; Jeon, I.-S.; Lee, M.-K.; Kim, N.-H.; Han, Y.-H.; Lee, S. *J. Phys. Chem. B* **2003**, *107*, 14109–14118.
- (25) Kassab, E.; Langlet, J.; Evleth, E.; Akacem, Y. *THEOCHEM* **2000**, 267.
- (26) Jensen, J. H.; Gordon, M. S. *J. Am. Chem. Soc.* **1995**, *117*, 8159–8170.
- (27) Fernandez-Ramos, A.; Smedarchina, Z.; Siebrand, W.; Zgierski, M. Z. *J. Chem. Phys.* **2000**, *113*, 9714.
- (28) Xu, S. J.; Nilles, J. M.; Bowen, K. H. *J. Chem. Phys.* **2003**, *119*, 10696.
- (29) Tajkhorshid, E.; Jalkanen, K. J.; Suhai, S. *J. Phys. Chem. B* **1998**, *102*, 5899–5913.
- (30) Blom, M. N.; Compagnon, I.; Polfer, N. C.; von Helden, G.; Meijer, G.; Suhai, S.; Paizs, B.; Oomens, J. *J. Phys. Chem. A* **2007**, *111*, 7309–7316.
- (31) Koyanagi, G. K.; Cheng, P.; Bohme, D. K. *J. Phys. Chem. A* **2010**, *114*, 241–246.
- (32) Shayesteh, A.; Lavrov, V. V.; Koyanagi, G. K.; Bohme, D. K. *J. Phys. Chem. A* **2009**, *113*, 5602–5611.
- (33) Feil, S.; Koyanagi, G. K.; Bohme, D. K. *Int. J. Mass. Spectrom.* **2009**, *280*, 38–41.
- (34) O'Brien, J. T.; Prell, J. S.; Steill, J. D.; Oomens, J.; Williams, E. R. *J. Am. Chem. Soc.* **2009**, *131*, 3905–3912.
- (35) Wu, R.; McMahon, T. B. *J. Am. Chem. Soc.* **2008**, *130*, 3065–3078.
- (36) Raspopov, S. A.; McMahon, T. B. *J. Mass. Spectrom.* **2005**, *40*, 1536–1545.
- (37) Wu, R.; McMahon, T. B. *J. Mass. Spectrom.* **2008**, *43*, 1641–1648.
- (38) Wu, R.; McMahon, T. B. *J. Am. Chem. Soc.* **2007**, *129*, 4864–4865.
- (39) Oh, H.-B.; Lin, C.; Hwang, H. Y.; Zhai, H.; Breuker, K.; Zabrouskov, V.; Carpenter, B. K.; McLafferty, F. W. *J. Am. Chem. Soc.* **2005**, *127*, 4076–4083.
- (40) Rajabi, K.; Fridgen, T. D. *J. Phys. Chem. A* **2008**, *112*, 23–30.
- (41) Prell, J. S.; Flick, T. G.; Oomens, J.; Berden, G.; Williams, E. R. *J. Phys. Chem. A* **2010**, *114*, 854–860.
- (42) Talley, J. M.; Cerda, B. A.; Ohanessian, G.; Wesdemiotis, C. *Chem. Eur. J.* **2002**, *8*, 1377–1388.
- (43) Dunbar, R. C.; Polfer, N. C.; Oomens, J. *J. Am. Chem. Soc.* **2007**, *129*, 14562–14563.
- (44) Armentrout, P. B.; Rodgers, M. T.; Oomens, J.; Steill, J. D. *J. Phys. Chem. A* **2008**, *112*, 2248–2257.
- (45) Cerda, B. A.; Wesdemiotis, C. *Analyst* **2000**, *125*, 657–660.
- (46) Polfer, N. C.; Oomens, J.; Dunbar, R. C. *Phys. Chem. Chem. Phys.* **2006**, *8*, 2744–2751.
- (47) Bush, M. F.; O'Brien, J. T.; Prell, J. S.; Saykally, R. J.; Williams, E. R. *J. Am. Chem. Soc.* **2007**, *129*, 1612–1622.
- (48) Polfer, N. C.; Oomens, J.; Moore, D. T.; von Helden, G.; Meijer, G.; Dunbar, R. C. *J. Am. Chem. Soc.* **2006**, *128*, 517–525.
- (49) Bush, M. F.; Oomens, J.; Saykally, R. J.; Williams, E. R. *J. Am. Chem. Soc.* **2008**, *130*, 6463–6471.
- (50) Strittmatter, E. F.; Lemoff, A. S.; Williams, E. R. *J. Phys. Chem. A* **2000**, *104*, 9793–9796.
- (51) Rodriguez-Santiago, L.; Sodupe, M.; Tortajada, J. *J. Phys. Chem. A* **2001**, *105*, 5340–5347.
- (52) Constantino, E.; Rodriguez-Santiago, L.; Sodupe, M.; Tortajada, J. *J. Phys. Chem. A* **2005**, *109*, 224–230.
- (53) Forbes, M. W.; Bush, M. F.; Polfer, N. C.; Oomens, J.; Dunbar, R. C.; Williams, E. R.; Jockusch, R. A. *J. Phys. Chem. A* **2007**, *111*, 11759–11770.
- (54) Lemoff, A. S.; Bush, M. F.; Williams, E. R. *J. Phys. Chem. A* **2005**, *109*, 1903–1910.
- (55) Marino, T.; Tuscano, M.; Russo, N.; Grand, A. *J. Phys. Chem. B* **2006**, *110*, 24666–24673.
- (56) Rodgers, M. T.; Armentrout, P. B.; Oomens, J.; Steill, J. D. *J. Phys. Chem. A* **2008**, *112*, 2258–2267.
- (57) Jockusch, R. A.; Price, W. D.; Williams, E. R. *J. Phys. Chem. A* **1999**, *103*, 9266–9274.
- (58) Kapota, C.; Lemaire, J.; Maitre, P.; Ohanessian, G. *J. Am. Chem. Soc.* **2004**, *126*, 1836–1842.
- (59) Remko, M.; Rode, B. M. *J. Phys. Chem. A* **2006**, *110*, 1960–1967.
- (60) Rogalewicz, F.; Hopilliard, Y.; Ohanessian, G. *Int. J. Mass Spectrom.* **2000**, *201*, 307–320.
- (61) Hopilliard, Y.; Rogalewicz, F.; Ohanessian, G. *Int. J. Mass Spectrom.* **2000**, *204*, 267–280.
- (62) Rogalewicz, F.; Hopilliard, Y.; Ohanessian, G. *Int. J. Mass Spectrom.* **2001**, *206*, 45–52.
- (63) Rogalewicz, F.; Hopilliard, Y.; Ohanessian, G. *Int. J. Mass Spectrom.* **2003**, *227*, 439–451.
- (64) Rajabi, K.; Easterling, M. L.; Fridgen, T. D. *J. Am. Soc. Mass Spectrom.* **2009**, *20*, 411–418.
- (65) Frisch, M. J. et al. *Gaussian 09*, revision A.01; Gaussian, Inc.: Wallingford, CT, 2009.
- (66) Kuchle, W.; Dolg, M.; Stoll, H.; Preuss, H. *Mol. Phys.* **1991**, *74*, 1245–1263.
- (67) Gorman, G. S.; Speir, J. P.; Turner, C. A.; Amster, I. J. *J. Am. Chem. Soc.* **1992**, *114*, 3986–3988.